Journal of Applied Polymer Science

Effects of Mixing Protocols on Impact Modified Poly(lactic acid) Layered Silicate Nanocomposites

Touffik Baouz,[1] Eda Acik,[2] Farouk Rezgui,[1] Ulku Yilmazer[2]

[1]Laboratoire des Matériaux Organiques, Faculté de Technologie, Département de Génie des Procédés, Université Abderrahmane Mira, Béjaia 06000, Algeria

[2]Chemical Engineering Department, Middle East Technical University, 06800, Ankara, Turkey

Correspondence to: U. Yilmazer (E-mail: yilmazer@metu.edu.tr)

ABSTRACT: Poly(lactic acid)/2 wt % organomodified montmorillonite (PLA/OMMT) was toughened by an ethylene-methyl acrylate-glycidyl methacrylate (E-MA-GMA) rubber. The ternary nanocomposites were prepared by melt compounding in a twin screw extruder using four different addition protocols of the components of the nanocomposite and varying the rubber content in the range of 5–20 wt %. It was found that both clay dispersion and morphology were influenced by the blending method as detected by X-ray diffraction (XRD) and observed by TEM and scanning electron microscopy (SEM). The XRD results, which were also confirmed by TEM observations, demonstrated that the OMMT dispersed better in PLA than in E-MA-GMA. All formulations exhibited intercalated/partially exfoliated structure with the best clay dispersion achieved when the clay was first mixed with PLA before the rubber was added. According to SEM, the blends were immiscible and exhibited fine dispersion of the rubber in the PLA with differences in the mean particle sizes that depended on the addition order. Balanced stiffness-toughness was observed at 10 wt % rubber content in the compounds without significant sacrifice of the strength. High impact toughness was attained when PLA was first mixed with the clay before the rubber was added, and the highest tensile toughness was obtained when PLA was first compounded with the rubber, and then clay was incorporated into the mixture. Thermal characterization by DSC confirmed the immiscibility of the blends, but in general, the thermal parameters and the degree of crystallinity of the PLA were not affected by the preparation procedure. Both the clay and the rubber decreased the crystallization temperature of the PLA by acting as nucleating agents. © 2014 Wiley Periodicals, Inc. J. Appl. Polym. Sci. **2015**, *132*, 41518.

KEYWORDS: mixing protocol; nanocomposite; organoclay; poly(lactic acid); rubber-toughening

Received 14 July 2014; accepted 14 September 2014

DOI: 10.1002/app.41518

INTRODUCTION

Biodegradable polymers have attracted much attention from both academic and industrial points of view owing to the growing environmental and social concerns brought about by the environmental impact of plastics wastes stemming from conventional petrochemical polymers.[1,2] Polylactic acid (PLA) as one of this class of polymers derived from renewable resources, competes well with many available synthetic polymers owing to its good mechanical and physical properties, biocompatibility, and ease of processability.[1,2] These attributes make it an outstanding candidate with high potential to substitute for petroleum-based polymers in various applications such as biomedical, packaging, automotive, and others.[1,3] However, because of its inherent brittleness and low toughness, this linear thermoplastic polyester needs some modifications to tackle these drawbacks and enlarge its application window. In this sense, various approaches were investigated for this goal such as copolymerization, plasticization, addition of organic/inorganic fillers, and melt-blending with either biodegradable or nonbiodegradable polymers.[1–10]

Toughening of PLA by flexible polymers has gained much attention.[1–10] To compensate the softening effect of the toughener, addition of nanofillers, mostly organomodified montmorillonite (OMMT), was considered to form nanocomposites.[11–17] It is generally known that the performance of toughened blends depends on various parameters such as components ratios and their properties, interfacial adhesion between the components, rubber particle size and shape, processing conditions and preparation methods, etc.[6,8] In this context, the effect of addition procedure on the performance and properties of ternary nanocomposites has been examined for many systems, including PA6/EPR-g-MA/OMMT,[18] LDPE/E-MA-GMA/OMMT,[19] PS/SEBS-g-MA/OMMT,[20] PET/E-MA-GMA/OMMT,[21] PP/PP-g-AA/EVA/OMMT,[22] and others.[23–26] Borah et al.[23] studied LLDPE/EMA/OMMT using three different compounding protocols and two types of OMMT. It was found that the morphology and the properties of

the nanocomposites were dependent on the blending sequence and on the type of the clay used. The Cloisite®25A clay migrated from the LLDPE phase to the EMA phase at a surprisingly high rate and the corresponding nanocomposites exhibited high impact strength as compared with the neat blend. However, Cloisite®30B clay was mainly located at the interface of LLDPE and EMA, and the compound exhibited low impact strength. In PA6/ABS/OMMT using SMA as a compatibilizer, the OMMT was preferentially located in the PA6 matrix in exfoliated state irrespective of the compounding mode, and the morphology of ABS dispersed phase was reported to be highly altered by the mixing sequence, which in turn affected the mechanical properties.[24] The X-ray diffraction (XRD) results of PA66/SEBS-g-MA/OMMT showed exfoliated structure regardless of the preparation order, whereas TEM observations indicated that OMMT location was affected by the mixing procedure.[25] Moreover, the OMMT in the matrix or at the interface was found in the exfoliated state, but the clay that was enclosed in the rubber was only intercalated as a result of the high affinity of clay to PA66, suggesting that clay dispersion cannot be determined solely on the basis of XRD, but needs to be complemented by visual tools such as TEM. Dasari et al.[26] concluded that for PA66/SEBS-g-MA/OMMT, it is beneficial in terms of impact strength to have the maximum amount of the exfoliated organoclay in the PA66 matrix, because the presence of OMMT in the rubber phase decreases its cavitation ability because of the stiffening effect of OMMT and accordingly it reduces the toughening efficiency.

To the best of the authors' knowledge, the effects of blending order of the components of rubber-toughened PLA nanocomposites have not been studied yet. The objective of this work is to investigate the effects of four different melt compounding protocols on the performance of rubber-toughened PLA nanocomposites. The structure and the morphology of the nanocomposites were observed by XRD, TEM and scanning electron microscopy (SEM), their mechanical performance was evaluated by tensile and impact tests, and their thermal characteristics were measured by differential scanning calorimetry (DSC).

EXPERIMENTAL

Materials

An injection grade PLA (PLI 005) resin, with a density of 1.25 g/cm^3 (ISO 1183) and a melting temperature in the range of 145–155°C was purchased from NaturePlast (Caen, France). The rubber modifier, Lotader® AX8900, an ethylene-methyl acrylate-glycidyl methacrylate terpolymer (E-MA-GMA) with an EMA and GMA contents of 24 and 8 wt %, respectively, was supplied by Arkema (Puteaux, France). The clay nanofiller was an OMMT, (Cloisite®30B), from Southern Clay Products (Gonzales, TX, USA). It is a natural montmorillonite modified with a quaternary ammonium salt. The cation of the organic modifier is methyl, tallow, bis-2-hydroxyethyl, quaternary ammonium (MT2EtOH) at a concentration of 90 mEq/100 g clay, and the anion is chloride. Hydrophilic Cloisite®30B was chosen as the organoclay, because it is more compatible with hydrophilic PLA in comparison to hydrophobic Cloisite®20A, Cloisite®25A, and Cloisite® 15A. It contains two hydroxyl groups that can react both with the carboxyl groups of PLA and epoxy groups of the impact modifier.

Compounding and Sample Preparation

In the nanocomposites, the weight percent of the rubber was varied in the range of 5–20 wt %, and the amount of clay was kept constant at 2 wt %. The nanocomposites were compounded using a fully intermeshing co-rotating twin screw extruder ($L/D = 24$) (Thermo Prism TSE 16 TC). The processing conditions were: screw speed = 250 rpm, feed rate = 25 g/min, and extruder zone temperatures of 150–170–170–170–170°C from the hopper to the die. The extruded rods were collected using a belt conveyor and air cooled at room temperature. Thereafter, the rods were pelletized and stored in sealed plastic bags and kept in desiccators. Specimens for different characterizations were prepared using a mini-injection molding equipment (DSM Xplore®) at cylinder and mold temperatures of 170 and 60°C, respectively. Before extrusion and injection processes, PLA, OMMT, and the prepared formulations were vacuum dried over night at 80°C and the rubber was dried at 45°C.

Four addition modes (PC-I, PI-C, CI-P, and ALL-S) were considered to investigate the effects of addition method of the components on the final structure and properties of the nanocomposites. In the first three modes: P, C, and I stand for PLA, clay, and the impact modifier, respectively. For instance, in the PC-I sequence, the PLA and the clay were compounded in the first extrusion process, and the rubber modifier was added to the obtained mixture in the subsequent second run. In the ALL-S, all of the ingredients of the nanocomposite were fed simultaneously into the hopper. Because in the first three modes of addition, at least two of the ingredients experienced extrusion twice; the All-S mixture was also extruded twice so that its components experience more or less the same thermal and mechanical history as for the other mixtures. Neat PLA was also extruded twice under the same conditions to serve as a control material. Hereafter, the materials are referred to according to their sample codes.

CHARACTERIZATION

XRD and Transmission Electron Microscopy (TEM)

A Rigaku D/MAX 2200/PC X-ray diffractometer operating in reflection mode was used to record the XRD patterns of the pristine OMMT powder and the nanocomposites. Diffractograms were acquired at room temperature with a step size of 0.02° from $2\theta = 1°$ to 10° and 1°/min scan rate using a CuKα X-ray radiation ($\lambda = 1.5418$ Å) generated at 40 kV and 40 mA. The interlayer spacing (d_{001}-reflection) of the OMMT nanosheets in the samples was derived from the peak position in the XRD diffractograms according to Bragg's law ($n\lambda = 2\ d\ \sin\theta$).

The dispersion state of the filler in the nanocomposites was assessed by TEM imaging using a FEI Tecnai® Spirit G^2 Biotwin transmission electron microscope operating at 80 kV in bright field mode (FEI Company, OR, USA). Ultrathin sections (70–80 nm) of the nanocomposites were produced from freeze-fractured impact test bars. Sections were cut at cryogenic temperature using Leica® EM UC6 ultra-microtome (Leica Microsystems, Wetzlar, Germany) equipped with a diamond knife.

SEM

A Jeol JSM-6400 (Jeol, Tokyo, Japan) low-voltage scanning electron microscope was used to examine the morphology of the prepared materials. The samples were obtained from

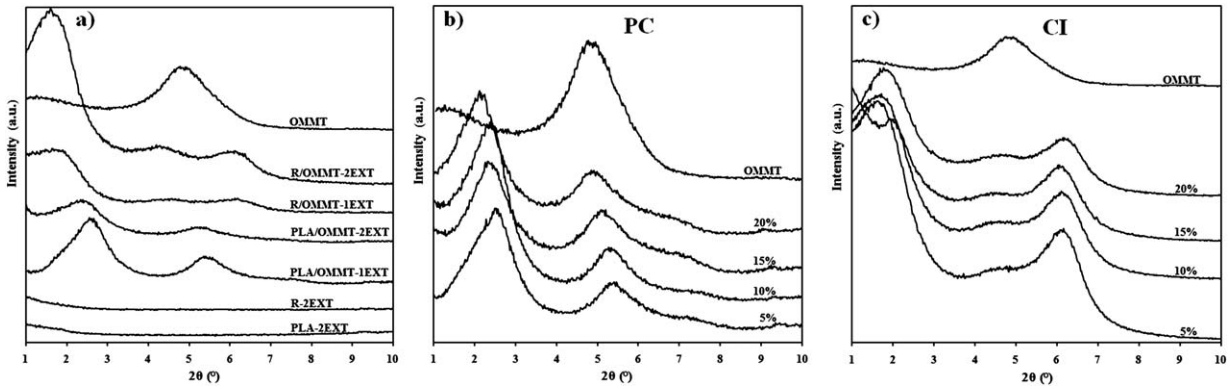

Figure 1. X-ray patterns of: (a) PLA, rubber, OMMT and their corresponding nanocomposites at 2 wt % OMMT, and (b) and (c) the PC and CI intermediate nanocomposites at different rubber contents, respectively. (The R indicates the rubber, and the percentages designate its wt %). The curves are shifted vertically for clarity.

cryofractured impact test bars. The etched surfaces, from which the rubber was selectively removed at 45°C using *n*-Heptane, were prepared with the aid of a sonicator. The surfaces were coated with a thin layer of gold to avoid electrostatic charging during observation. The impact modifier droplet size in all of the formulations was evaluated by the image processing software "ImageJ" (Rasband, W.S., ImageJ, U. S. National Institutes of Health (NIH), Bethesda, Maryland, USA, http://imagej.nih.gov/ij/, 1997–2011). Typically, a number of particles (approximately 250–300) from three to four independent SEM micrographs were analyzed by the program to estimate first the average area (A_i) of each individual particle (i). This obtained cross-sectional area (A_i) was then converted into equivalent diameter (d_i) of a sphere using eq. (1), and the number-average particle diameter (D_n) was computed by using eq. (2).

$$d_i = 2\sqrt{(A_i/\pi)} \tag{1}$$

$$D_n = \frac{\sum n_i d_i}{\sum n_i} \tag{2}$$

where n_i is the number of the dispersed domains having the apparent particle diameter d_i counted from the SEM images.

Thermal Characterization (DSC)

Thermal properties of the materials were investigated with the aid of a Shimadzu DSC-60 differential scanning calorimeter (DSC) (Shimadzu, Tokyo, Japan). The samples (9–10 mg) were heated from room temperature to 200°C at a heating rate of 10°C/min under constant nitrogen flow of 50 mL/min. The following events were determined from this scan: the glass transition temperature (T_g), crystallization temperature (T_c), melting temperature (T_m), crystallization enthalpy (ΔH_c), and melting enthalpy (ΔH_m).

The degree of crystallinity (χ_c) of PLA in the compounds was estimated using the following equation:

$$\chi_c\% = \left(\frac{\Delta H_m - \Delta H_c}{\Delta H_f \times \varphi_{\mathrm{PLA}}}\right) \times 100 \tag{3}$$

Where χ_c (%) is the degree of crystallinity, ΔH_m and ΔH_c are the heats of fusion and crystallization of the sample, respectively. ΔH_f is the heat of fusion of 100% crystalline PLA, and φ_{PLA} is the weight fraction of the PLA in the sample.

Mechanical Properties

Mechanical performance of the materials was investigated at room temperature. Tensile properties (Tensile modulus, tensile strength, and elongation at break) were determined according to ISO 527 at strain rate of 0.1 min^{-1} using a Shimadzu Autograph AG-IS 100 KN universal testing machine (Shimadzu, Tokyo, Japan). Unnotched Charpy impact strength (IS) measurements were assessed by using a Ceast Resil Impactor pendulum following the ISO 179 standard. At least five samples were tested for each property, and the values were averaged and reported together with their respective standard deviations.

RESULTS AND DISCUSSION

XRD Analyses

XRD patterns of the PLA and the rubber did not show any characteristic basal diffraction peak in the studied range of $2\theta = 1$–$10°$. However, the pure OMMT powder displayed a single strong characteristic peak at $2\theta = 4.78°$ ($d = 18.49$ Å) [OMMT in Figure 1(a)].

The characteristic peak of the OMMT in the binary PLA/OMMT nanocomposite extruded once was shifted to a lower angle $2\theta = 2.56°$ ($d = 34.51$ Å) [PLA/OMMT-1EXT in Figure 1(a)]. This indicates intercalation of the PLA molecules between the clay galleries, attributed to the favorable interactions of the PLA carboxyl (COOH) end groups with the hydroxyl entities of the clay surfaces and those of its surfactant.[6,12,19] Another OMMT peak with low intensity was observed at a higher angle $2\theta = 5.36°$ ($d = 16.49$ Å) than that of pure clay, because of the presence of tactoids [PLA/OMMT-1EXT in Figure 1(a)]. Clays are generally modified with an excess of surfactants,[27] thus the decrease in the original interlayer spacing of the OMMT is believed to be due to the collapse of the clay galleries resulting from the dissolution of some surfactant parts from clay galleries into polymer matrix[22,23] and/or to rearrangement of the alkyl ammonium chains of the OMMT.[19] When PLA/OMMT was extruded twice, the intensity of its two characteristic peaks was decreased and the peaks were shifted to lower angles $2\theta = 2.34°$ ($d = 37.75$ Å) and $2\theta = 5.16°$ ($d = 17.13$ Å) owing to the longer

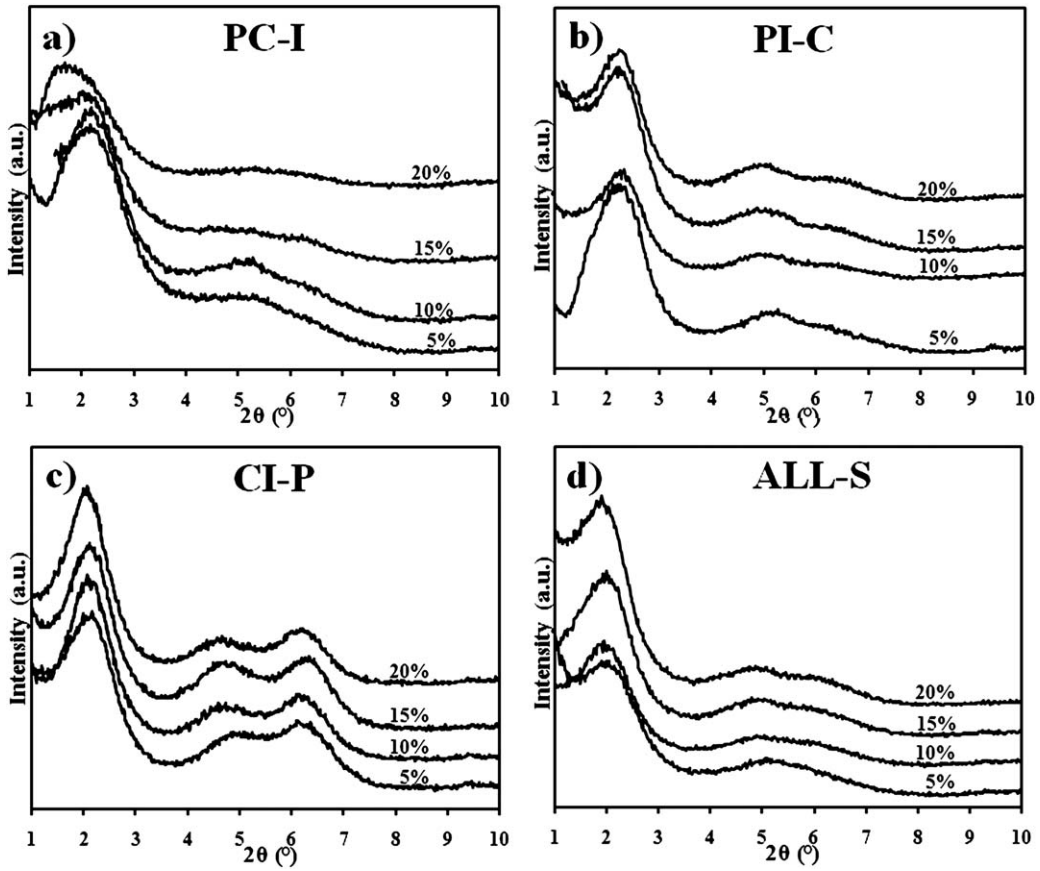

Figure 2. X-ray diffractograms of: (a) PC-I, (b) PI-C, (c) CI-P, and (d) ALL-S nanocomposites prepared at various rubber contents. The curves are shifted vertically for clarity.

residence time of the nanocomposite in the extruder, that caused longer duration of shear and interactions between reactive groups of PLA and those of the clay surfaces and its surfactant [PLA/OMMT-2EXT in Figure 1(a)].

The rubber-based nanocomposite extruded once (R/OMMT-1EXT) exhibited three characteristic peaks on its diffractogram recorded at $2\theta = 1.64°$ ($d = 53.87$ Å), $2\theta = 4.48°$ ($d = 19.72$ Å) and $2\theta = 6.12°$ ($d = 14.44$ Å) [R/OMMT-1EXT in Figure 1(a)]. This indicates low intercalation degree of the rubber owing to its higher molecular weight (high viscosity) and lower polarity (lower affinity to clay) compared with PLA, and to its bulky GMA groups making its intercalation into clay interlayers difficult. Subjecting this nanocomposite to a second extrusion process did not improve the dispersion of clay, because its X-ray traces revealed the same peaks at the same positions [R/OMMT-2EXT in Figure 1(a)].

To get more insight into the intercalation process, the difference between the rubber and the PLA, the PC and CI intermediate nanocomposites were also studied. The PC nanocomposites showed the two PLA/OMMT characteristic peaks of nearly the same intensities shifted to lower angles that varied from $2\theta = 2.50°$ ($d = 35.34$ Å) to $2\theta = 2.12°$ ($d = 41.67$ Å) and from $2\theta = 5.40°$ ($d = 16.37$ Å) to $2\theta = 4.84°$ ($d = 18.26$ Å) as the clay level increased suggesting improved clay dispersion [Figure 1(b)]. The CI nanocomposites exhibited three peaks as those of the R/OMMT-1EXT situated at almost the same positions $2\theta = 1.58°$ ($d = 55.91$ Å), $2\theta = 4.38°$ ($d = 20.17$ Å) and $2\theta = 6.10°$ ($d = 14.49$ Å) indicating nearly identical clay dispersion for all the clay contents [Figure 1(c)]. The peak at $2\theta = 6.10°$ points out to the appreciable collapse of the clay galleries, the intensity of which decreases as the clay content decreases. These results show that PLA intercalates better than the rubber for the same reasons stated earlier.

Figure 2(a–d) depicts the clay dispersion in each blending mode. As it can be seen on this figure, all of the addition sequences studied led to intercalated/partially exfoliated nanostructures. Considering PC-I, the addition of 5 wt % rubber to the PC nanocomposite shown in Figure 1(b), shifted its two peaks from $2\theta = 2.50°$ ($d = 35.34$ Å) and $2\theta = 5.40°$ ($d = 16.37$ Å) to $2\theta = 1.98°$ ($d = 44.62$ Å) and $2\theta = 5.16°$ ($d = 17.13$ Å) [Figure 2(a)]. As the rubber content increased, the dispersion of clay was enhanced and better intercalated/partially exfoliated structures are observed at and above 15 wt % rubber ratio with absence of tactoids. Indeed, at 20 wt % rubber fraction, the peak at the highest diffraction angle nearly disappeared and the second one is shifted to $2\theta = 1.76°$ ($d = 50.19$ Å). This suggests additional intercalation of the rubber into the basal spacing of the clay where PLA chains had already penetrated.[6,14] This occurs due to

the viscosity build up imparted by the rubber to the system that promoted high shear intensity favoring more clay nanoplatelet delamination.[6,19–22] In addition, in the PC-I sequence, both PLA and clay experienced extrusion twice contributing to improved clay dispersion by promoting more PLA molecules to diffuse into the clay spacings. In addition, this fine clay dispersion arose due to the polar interactions of the rubber and PLA ester groups, and to the chemical reaction between the rubber epoxy moieties with terminal (COOH) and (OH) groups of the PLA[3–8] and with the (OH) groups of the clay surfaces and those of its surfactant. The reactions of the (COOH) and (OH) groups with the epoxy groups were identified by FTIR by Yeh et al.[3] and Juntuek et al.[4] The schematic representation of these reactions was published by Sun et al.,[5] and their mechanism in the presence of a catalyst was discussed by Oyama et al.[28]

For PI-C nanocomposites, when the rubber extent was 5 wt %, the OMMT diffraction peak shifted to lower angle $2\theta = 2.10°$ ($d = 42.07$ Å), which remained at almost the same position for all the rubber contents [Figure 2(b)]. The second peak recorded at $2\theta = 5.12°$ ($d = 17.26$ Å) indicate that there are remaining tactoids in 5 wt % PI-C nanocomposite. At 10 wt % rubber content, the intensities of the peaks decreased and the peak at $2\theta = 5.12°$ ($d = 17.26$ Å) shifted to $2\theta = 4.90°$ ($d = 18.03$ Å) pointing out to better dispersion. At 20 wt % rubber content, in addition to the two peaks detected at the same positions as in the 10 wt % nanocomposite, a third peak at $2\theta = 6.42°$ ($d = 13.77$ Å) appeared. The third peak indicates low clay dispersion state owing to the chain extension induced by the reaction between the PLA and the rubber functional groups restricting the chain mobility of the PLA and the rubber molecules to enter into the clay galleries.[3,5–9,11] PI-C exhibited lower clay dispersion levels compared with PC-I, because the interactions between the PLA and the rubber were maximized during the first extrusion step (formation of PI) which reduced the total reactive groups of the polymers to interact with the clay. In addition, in the PI-C mixing order the clay was mixed only once with the polymers.

All diffractograms of CI-P nanocomposites exhibited nearly the same trend with three distinct peaks positioned at the same diffraction angles regardless of the rubber ratio implying almost the same clay dispersion in these nanocomposites [Figure 2(c)]. In these mixtures, both intercalation and re-agglomeration of previously dispersed clay in the CI compounds took place. The peak at $2\theta = 6.10°$ ($d = 14.49$ Å) was observed at the same position as in CI compounds but with lower intensities associated with reduced amount of tactoids owing to the additional intercalation by the added PLA into the clay galleries. The two peaks at $2\theta = 1.58°$ ($d = 55.91$ Å) and $2\theta = 4.38°$ ($d = 20.17$ Å) in CI mixtures increased in intensity and shifted to higher angles located at $2\theta = 2.10°$ ($d = 42.07$ Å) and $2\theta = 4.66°$ ($d = 18.96$ Å) when PLA was incorporated, suggesting the collapse of clay interlayers and/or re-agglomeration of the already expanded nanofiller in the CI compounds. Note that in this mixing mode, CI mixtures were extruded twice which was found to be deleterious on the dispersion of the clay as discussed previously in the case of R/OMMT-2EXT [Figure 1(a)]. This fact explains the deterioration of the clay dispersion state when PLA was added in the second extrusion step to form CI-P nanocomposites.

Figure 2(d) shows the XRD patterns of the ALL-S extruded twice. It can be noticed that the diffractograms resemble those obtained for PI-C compounds but with diffraction angles shifted to lower angles with lower intensities designating better dispersion than that of PI-C. OMMT peak was shifted to $2\theta = 1.90°$ ($d = 46.50$ Å) for all of the ALL-S nanocomposites, and the remaining tactoids were identified at $2\theta = 5.10°$ ($d = 17.33$ Å) and at $2\theta = 4.90°$ ($d = 18.03$ Å) when the rubber fraction was 5 and 20 wt % respectively with the appearance of a third peak at $2\theta = 5.90°$ ($d = 14.98$ Å) for this last composition. The highest level of dispersion is observed at 10 wt % rubber content with diffraction angles positioned at $2\theta = 1.90°$ ($d = 46.50$ Å) and $2\theta = 4.78°$ ($d = 18.49$ Å).

Better clay dispersion is exhibited in ALL-S nanocomposites compared with that of PI-C, because all the ingredients in ALL-S were fed at the same time into the extruder and were processed twice, consequently the interactions between the three ingredients were maximized. However, in PI-C the interactions between polymers were favored in the first extrusion step (PI), and the intercalation process was only accomplished during the second run which had affected the extent of dispersion owing to the short interaction time of the OMMT with the polymers.

TEM Analyses

Selected TEM photomicrographs of the nanocomposites are shown in Figures 3 and 4. All images attest to the formation of nanocomposites with structural characteristics consistent with the XRD analyses. In these micrographs, the base background represents the matrix, the dark lines and darker entities are the clay nanoplatelets and their stacks successively.

TEM photomicrograph at low magnification of PLA/OMMT nanocomposite reveals that clay nanosheets were uniformly and randomly dispersed in the PLA [Figure 3(a)]. Upon zooming to a higher magnification, the TEM image of this binary mixture displays a hybrid structure composed of intercalated/partially exfoliated clay with numerous individual isolated silicate nanoplatelets and coexistence of thin primary clay tactoids [Figure 3(b)]. Such structure originated, as aforementioned, from the strong interactions between PLA terminal groups and hydroxyl entities of OMMT nanoplatelet surfaces and of its ammonium surfactant. These visual observations are in close accordance with the XRD results on PLA/OMMT.

Unlike PLA/OMMT, the R/OMMT extruded twice (R/OMMT-2EXT) exhibits poor dispersion manifested by the occurrence of close clustered clay groups [Figure 3(c)]. Its TEM image at high magnification clearly demonstrates intercalated/partially exfoliated clay structure with slight amount of delaminated nanosheets and thick tactoids indicative of incomplete exfoliation [Figure 3(d)].

The structure of PC nanocomposite consists of abundant single exfoliated clay nanosheets and intercalated/partially exfoliated regions and thin clay stacks [Figure 3(e)], whereas that of CI is

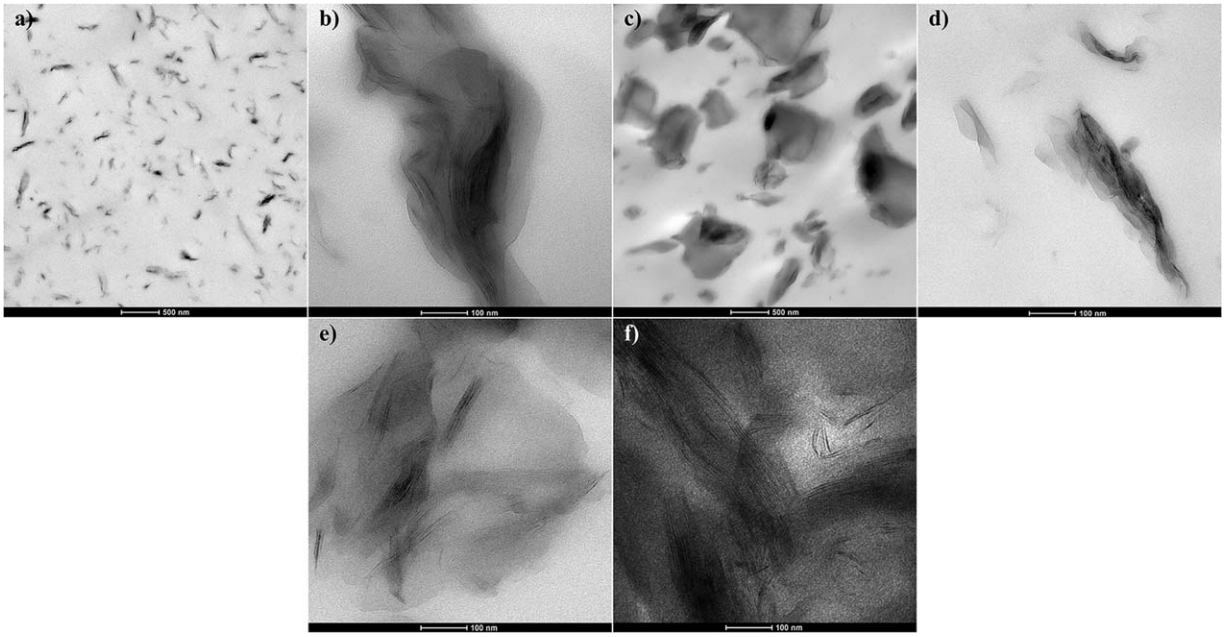

Figure 3. TEM micrographs at low and high magnification of (a, b) PLA/2 wt % OMMT and (c, d) R/2 wt % OMMT, respectively, and TEM micrographs at high magnification of (e) PC and (f) CI intermediate nanocomposites.

mainly made of intercalated structure and few exfoliated particles with occurrence of large number of thick clay stacks and tactoids which can be assimilated to agglomerates of different sizes [Figure 3(f)].

The TEM analyses of these four nanocomposites (PLA/OMMT, R/OMMT, PC, and CI) are in good agreement with the diffraction peaks appearing in their XRD patterns confirming that clay particles are more dispersed in PLA than in the rubber as a result of the disparity in their polarities and hence their affinity to clay.

Representative high magnification TEM micrographs of the ternary nanocomposites prepared by different addition protocols are exhibited in Figure 4. Owing to the absence of contrast between the PLA and the rubber, it is difficult to differentiate between the two polymer phases and thus to locate the clay. For the sake of brevity only the micrographs of the nanocomposites at the optimal 10 wt % rubber ratio are shown, because at this composition the best stiffness-toughness balance has been acquired, especially for PC-I and PI-C mixing sequences.

The main common observation for PC-I, PI-C and ALL-S is that they all show a nanoscale dispersed morphology dependent on rubber composition identified by the presence of single clay nanosheets without appearance of any agglomeration, whereas for the CI-P nanocomposite, the rubber content did not significantly influence the nanoscale clay dispersion, and discrete agglomerates constituted most of the structure. In all preparation procedures, the OMMT particles were dispersed without any obvious orientation preference, and none of them led to completely exfoliated nanocomposite.

PC-I presented the highest level of clay dispersion [Figure 4(a)]. Exfoliated clays constitute the major structure evidenced from single clay nanoplatelets, thin stacks and absence of tactoids. Such high dispersion degree was possible because the favorable reactions between the PLA reactive groups and those on the clay took place for a longer time (PC mixture was extruded

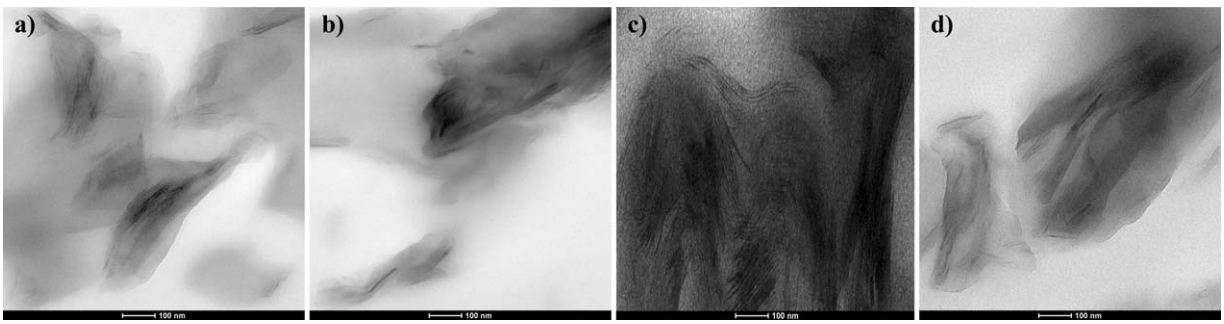

Figure 4. TEM photomicrographs of: (a) PC-I, (b) PI-C, (c) CI-P, and (d) ALL-S nanocomposites prepared at 10 wt % rubber content.

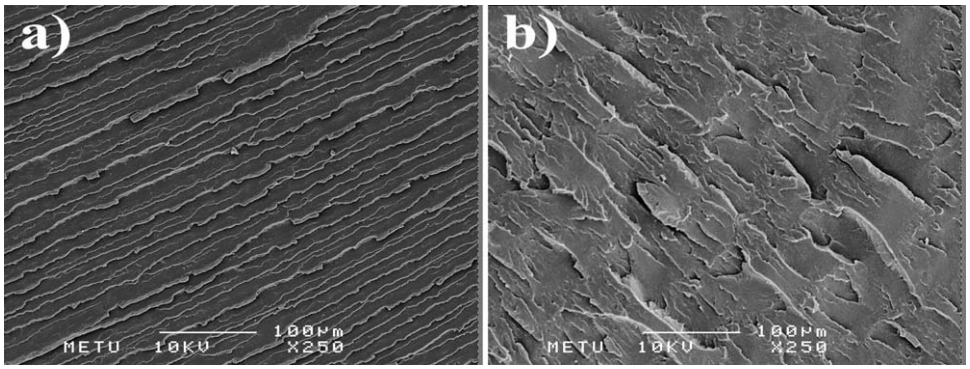

Figure 5. SEM micrographs of the cryofractured surfaces of the injection molded specimens of (a) PLA and (b) PLA/2 wt % OMMT.

twice). Furthermore, the shear melt viscosity became high in the second extrusion step induced by the added viscous rubber that improved delamination and breakdown of clay tactoids and helped insertion of both types of polymer molecules into the clay stacks as was confirmed by XRD.

PI-C TEM micrograph exhibits lower dispersion level than PC-I [Figure 4(b)]. This image shows intercalated structures, some single nanoplatelets and thin stacks, and slight amount of tactoids. This is the result of the interactions between the polymers in the first extrusion run that reduced the available reactive groups of the polymers to interact with the clay, and also the intercalation could only take place in the second extrusion run (short residence time).

CI-P nanocomposite presented the worst clay dispersion state, characterized by intercalated clay particles, large amount of clay tactoids, agglomerates and almost total absence of exfoliated clay particles Figure 4(c). This structure was the result of the low diffusion ability of the rubber into clay interlayers during the extrusion of CI mixture, and to its possible bonding to clay edges through interactions of its reactive groups with the hydroxyl groups of the clay surfaces that prevented the rubber and the PLA to intrude further into clay galleries during the second extrusion step.[6] The deleterious effect of extruding CI intermediate nanocomposite twice on clay dispersion was discussed earlier in the XRD section. Another factor that could also be considered is the presence of clay agglomerates that constrained the motion of the polymer chains necessary for their diffusion into clay galleries.[6,11–13,20,23] These agglomerates stemmed from encapsulation of most of the clay by the rubber that enhanced platelet-platelet interactions, and the extensive shear forces applied by extrusion were not able to breakdown these agglomerates. In addition, collapse of the clay galleries were triggered by the high shear intensity during CI extrusion. Dissolutions of the organoclay surfactant into the matrix during processing has been well documented in the literature.[6,12,16]

ALL-S presents finer clay dispersion in comparison to that of PI-C, consisting of intercalated particles and myriad single clay particles, thin clay stacks and few tactoids [Figure 4(d)]. This finer dispersion compared with PI-C is the result of the competition between the rubber and the PLA to react and to simultaneously enter within the clay galleries. Moreover, in this mixing order, the ingredients were in contact for longer time (two extrusion processes), thus giving more and equal chances for both polymers to diffuse into the clay galleries.

Morphology (SEM) Analyses

Illustrative SEM micrographs of the freeze fractured surfaces of twice extruded PLA and PLA/OMMT are shown in Figure 5. PLA displays a typical brittle fracture surface as shown by a smooth surface and several parallel straight cracks developed throughout the surface [Figure 5(a)]. Absence of crack deflections ascribed to the homogeneous structure of PLA led to rapid crack growth and abrupt breaking of PLA with low fracture resistance and observable stress whitening on the specimens that might explain the low impact toughness of PLA.[19] PLA/OMMT SEM micrograph [Figure 5(b)], shows a rough surface compared with PLA attributed to the effective ability of clay nanoplatelets in diverting cracks in random directions giving rise to numerous short and long crack paths responsible of such feature.[6,29] Such mechanism was possible owing to the produced OMMT intercalated/partially exfoliated structure coupled with the valid interactions between the functional groups of the PLA and the clay that enabled improved load transfer from the matrix to the reinforcement.[6,11,12,19]

Figure 6(a–d) exhibits representative SEM images of unetched cryofractured surfaces of the ternary nanocomposites at 10 wt % rubber content. Intense macroscopic stress whitening compared with PLA and PLA/OMMT was noticed on all impacted specimen surfaces that confirm improvement of toughness. All SEM images exhibited a two-phase morphology. This morphology is typical of an immiscible polymer system, in which the rubber composed the dispersed phase surrounded by the continuous PLA matrix. The interface is not clear indicating strong adhesion between the phases derived from the *in situ* interfacial reaction between the functional terminal groups of the PLA and those of the elastomer giving rise to *in situ* formed PLA-g-rubber copolymer that strengthened the interface by bridging the two phases for adequate load transfer.[2,6,11,12,19,27,28] This was identified by the deformation of the domains into ellipsoids and their enlargement in the stress direction demonstrating that the rubber shared the load with the matrix. The presence of this copolymer at the interface simultaneously decreased the interfacial tension and droplet coalescence rate through steric repulsion between the copolymer

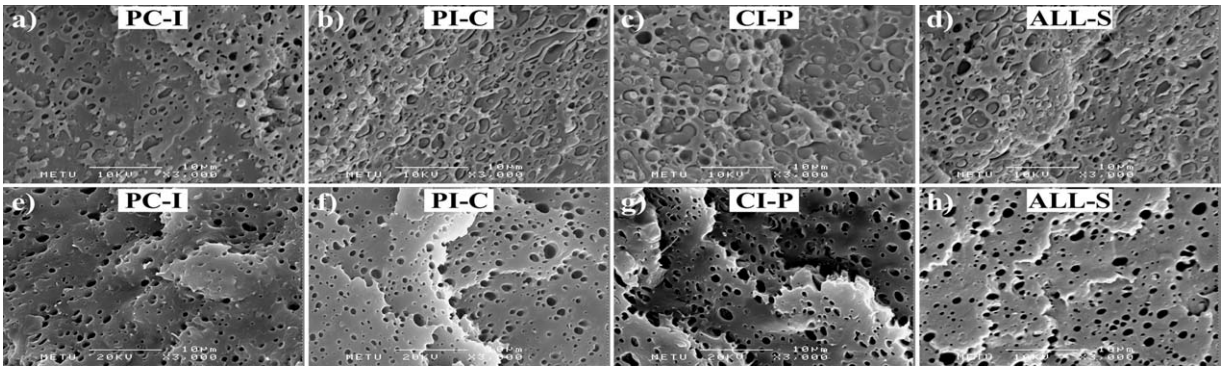

Figure 6. SEM micrographs of the fractured injection molded specimens of (a–d) unetched surfaces, and (e–h) etched surfaces of the ternary nanocomposites all with 10 wt % rubber content.

molecules and promoted droplet breakup rate hence resulting in fine particle size dispersion.[4–6,24,27,28] Furthermore, these micrographs present some vacuoles corresponding to pulled-out rubber droplets during impact, whereas others were well anchored to the matrix and some were still embedded within the PLA matrix enveloped by micro-voids. These gaps might have resulted from the debonding and/or cavitation of the rubber particles at the interface.[2,7–11,15,30] Debonding/cavitation of rubber particles is one of the most important mechanisms of energy absorption in rubber-toughened polymers among others, such as crazing, internal rubber cavitation, shear banding, crack bridging and shear yielding, all of which are highly influenced by particle size and interface strength.[7,30]

The morphology of etched fractured surfaces of selected ternary nanocomposites at 10 wt % rubber content is shown in Figure 6(e–h). The craters on the photographs correspond to the location of the rubber particles extracted by chemical etching. All of the nanocomposites present fine phase structures. Figure 6(e–h) shows that during impact, fracture surfaces with higher surface roughness than that of PLA/OMMT [Figure 5] were generated. This indicates that much energy has been consumed to create these surfaces and shows that the transition from brittle (crazing) to tough (shear yielding) fracture took place mainly by cavitation induced shear yielding.[2,7–11,15,30]

At low rubber fraction, droplet breakup is favored against coalescence, owing to the low rubber concentration (low viscosity) and to decreased interfacial tension between the components imparted by the *in situ* formed copolymer at the interface. As a result, small particles are formed with narrow and homogeneous distribution, but at higher rubber contents, during mixing the domain size is determined by the competition between particle breakup and coalescence.[6,28] Moreover, the particle size could also be influenced by the presence of OMMT that generally induces a change in the phase size depending on its location.[6,20,22–27]

PC-I presented the lowest domain size (253–434 nm) because of the presence of most of the clay nanosheets predominately in the matrix that might have acted as physical obstacles to coalescence of the rubber particles[6,11–13,27] [Figure 6(e)]. Some of the clay may also have migrated to the interface.[16,22–24,26,27] Martins et al.[22] reported in their study of PP/PP-g-AA/EVA/OMMT nanocomposites that the clay migrated to the EVA phase by affinity, irrespective of the blending order, even in the sequence where the clay was first mixed with polypropylene, before EVA was added. Similarly, Borah et al.[23] observed that in LLDPE-g-MA compatibilized LLDPE/EMA/OMMT nanocomposites, the OMMT (Cloisite®25A) was attracted to the EMA phase by affinity during the short residence time in the internal mixer even though the clay was previously mixed with the molten polyethylene and EMA was added subsequently. The presence of the clay at the PLA/rubber interface in PC-I nanocomposite might have constituted physical hindrance for coalescence of the rubbery domains, accordingly small rubber domains are generated.[6,11–13,18,20,23,24,27]

The rubber droplet size of PI-C (333–545 nm) [Figure 6(f)] is somewhat larger than that of PC-I. In this nanocomposite, the clay was added in the second extrusion run, consequently it should be distributed in the two phases, with preference for PLA owing to the higher polarity of PLA in comparison to the rubber. Dasari et al.,[25,26] reported that the clay was equally dispersed in PA66 and SEBS-g-MA when they used PI-C addition mode to prepare the PA66/SEBS-g-MA/OMMT nanocomposite. The presence of the clay in the rubber phase increased the modulus of the rubber and hence reduced its ability to breakup compared with PC-I mixing order.[24–27] This effect coupled with the increased viscosity of the system due to the chain extension reaction decreased droplet breakup during blending. Both of these factors might have reduced the compatibilizing effect of the clay and hampered its physical barrier behavior for coalescence, therefore in the PI-C mixing sequence larger particles were developed compared with PC-I.

For CI-P and ALL-S, most of the clay should be present in the dispersed phase. In the case of CI-P this is evident because the clay is first mixed with the rubber. For ALL-S, during blending the rubber melted earlier (T_m ≈53°C) than PLA did (T_m ≈147°C), therefore most of the clay should also be enclosed in the rubber. However, in both cases, some of the OMMT might be present at the PLA/rubber interface and/or in the PLA phase. This preferential location of OMMT in the elastomer phase increased the viscosity and modulus of the rubber, accordingly the droplet deformation and breakup during blending were considerably reduced leading to larger domain size in these

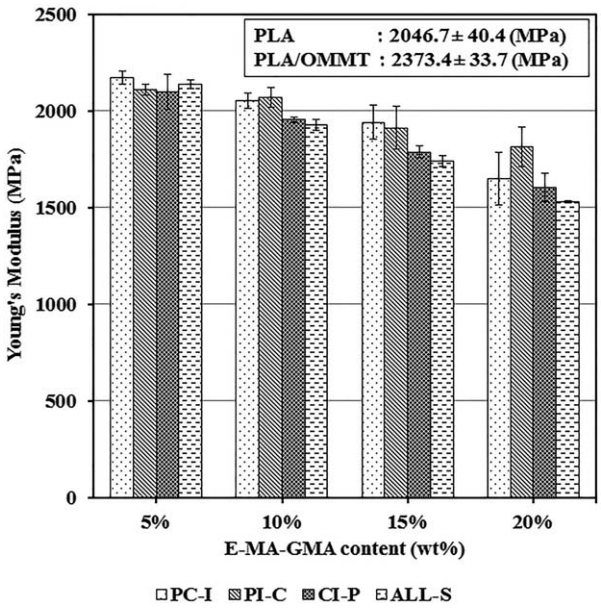

Figure 7. Young's modulus of the ternary nanocomposites as a function of the rubber content at 2 wt % clay.

nanocomposites in comparison to those of PC-I and PI-C. The domain size of ALL-S [Figure 6(g)], and CI-P [Figure 6(h)] were (449–689 nm) and (457–1524 nm) respectively. ALL-S exhibited smaller phase size than CI-P did, because all of its ingredients were extruded twice and the elastomer droplets were broken up during the early stages of their formation. However, CI-P was prepared from the highly viscous CI intermediate compound that was difficult to extrude and to disperse into PLA; therefore, larger particles were produced in this nanocomposite.

In all the mixing methods, the domain size increased with increasing rubber content (not shown here).[3,6,10,20] This is an expected result, as the rubber fraction increases the viscosity of the system and the tendency of particle collision and agglomeration increases, consequently the coalescence rate becomes higher than the droplet breakup rate, resulting in larger particle size.[20] In this study, particularly for PC-I and PI-C, at higher rubber ratio, the coalescence suppression and the compatibilizing effects of the clay were not significant probably due to its low concentration (2 wt %).

Mechanical Properties

Stress–strain curves of the studied materials (not shown here) were determined at room temperature. Upon drawing, PLA exhibited a sharp linear increase in stress with a distinct yield point accompanied thereafter by a short necking and an abrupt rupture at low strain (3.9%), demonstrating its brittleness and its low tensile toughness. Addition of 2 wt % OMMT to PLA did not bring about a noticeable change to the PLA deformation behavior. However, for all the compounding modes, incorporation of the rubber to the nanocomposites transformed the fracture of PLA from brittle to ductile. During stretching, these modified nanocomposites exhibited a broad yield peak and a long stable necking after which the strain increased considerably and continuously at nearly constant stress indicative of plastic flow (cold drawing), followed by a short stress softening before failure. The failure occurred at a significantly increased elongation at break signifying that high energy was dissipated.

Figures 7–9 display the tensile properties namely tensile modulus, tensile strength and elongation at break as a function of rubber loading for each of the considered mixing protocol. For the sake of comparison, the results for PLA and its corresponding nanocomposite (PLA/OMMT), both of them extruded twice, are written on each graph.

Tensile Modulus

The Young's modulus of neat PLA and those of the PLAs extruded once and twice were 2149.0, 2068.0, and 2046.7 MPa, respectively. There was no substantial change of PLA modulus with reprocessing, which is in line with published results in the literature.[31,32] Tensile modulus of PLA was found to remain constant after seven injection cycles,[31] and 10 extrusion processes.[32]

In the presence of 2 wt % OMMT, the tensile modulus of PLA increased from 2046.7 to 2373.4 MPa [Figure 7]. This is a common outcome attributed to the replacement of PLA molecules with OMMT that has high intrinsic stiffness and high aspect ratio.[6,11,12,16–20,23–27] This increase is correlated with the high level of OMMT dispersion (as was assessed by XRD and TEM) that increased the clay-polymer contact surface area and its effective volume fraction, thus imposing restrictions on chain mobility and deformation of the surrounding matrix.[6,11–13,18,20,23–27] In addition to these effects, the strong adhesion through interfacial interactions of PLA carboxyl end groups and the hydroxyl entities of the nanoclay contributes to efficient stress transfer from the polymer matrix to the filler giving rise to high tensile modulus of the PLA/OMMT nanocomposite.

As documented in Figure 7, for all the blending sequences the modulus dropped steadily as the rubber quantity is increased owing to the soft nature of the rubber with low modulus.[1–8,10,11,13–16,18,19,21–26] When the elastomer was added at 5 wt %, the modulus decreased from 2373.4 MPa to approximately 2100.0 MPa for all the nanocomposites, but at 10 wt % rubber content, the Young's modulus was more or less retained, especially for PC-I and PI-C mixing orders. Above this rubber content, PC-I and PI-C still displayed the highest modulus that might be due to the fine dispersion of the OMMT in the PC-I mixing order that contributed to chain immobilization, responsible of increased chain stiffening. For the PI-C mixing order, the increase might be ascribable not only to the fine clay dispersion, but also to promoted chain extension associated with significant reaction extent between the functional groups of PLA and those of the impact modifier that increased the molecular weight, and resulted in more stabilized and strengthened interface.

For the CI-P and ALL-S mixing orders, the OMMT was mostly present in the elastomer phase as discussed in TEM section. This indicates that encapsulation of the clay layers by the rubber phase has an adverse effect on their stiffening effectiveness.

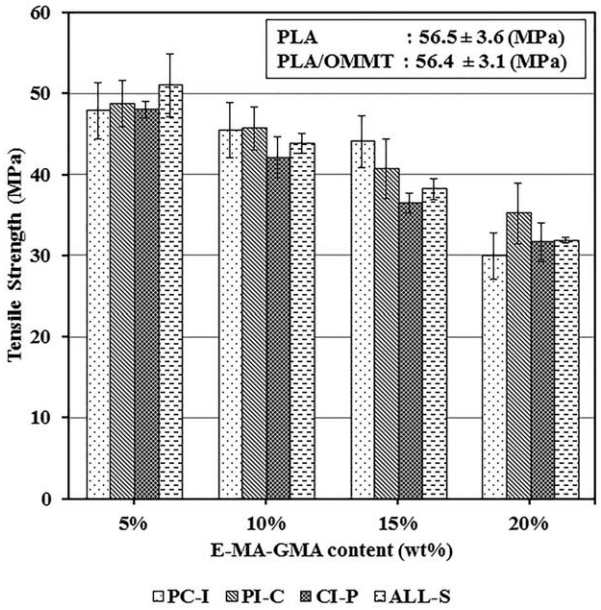

Figure 8. Tensile strength of the ternary nanocomposites as a function of the the rubber content at 2 wt % clay.

Tensile Strength

PLA showed a high tensile strength of 56.5 MPa [Figure 8]. No significant change of this property was distinguished after addition of 2 wt % OMMT to PLA. The nanocomposite exhibited intercalated/partially exfoliated nanostructure which should facilitate the stress transfer between the phases. However, the tensile strength of the material is strongly dependent on the orientation of the clay layers, and if the clay layers in the tensile bar are not preferentially oriented in the testing direction the increase in the tensile strength would be minimal.

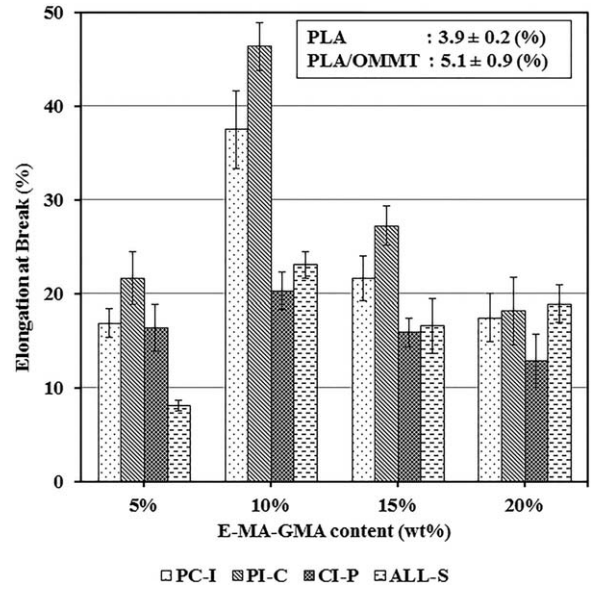

Figure 9. Elongation at break of the ternary nanocomposites as a function of the rubber content at 2 wt % clay.

The tensile strength as a function of the rubber ratio followed the same trend as that of the tensile modulus [Figure 8]. It decreased as the elastomer fraction was increased, regardless of the compounding protocol which is again attributed to the elastomeric nature of the rubber. This reduction in the tensile strength is consistent with previous research that reported reduced tensile strength in rubber-toughened PLA blends[1–4,6,10,11,13,15–17] and in other toughened polymer blends.[18–20,23]

At 5 wt % rubber content, the tensile strength was almost retained at 49.0 MPa independent of the compounding order, as a result of the somewhat similar OMMT dispersion level developed at this rubber ratio in all the compounding sequences. At this low rubber content, the location of the clay in the nanocomposites did not significantly affect the tensile strength, and the presence of clay agglomerates in the CI-P nanocomposite was not so detrimental. At 10 wt % rubber concentration, the tensile strength of all the nanocomposites underwent approximately the same decrease.

At 15 wt % elastomer content, the high tensile strengths of PC-I and PI-C compared with those for CI-P and All-S can be attributed to the presence of most of the clay in the PLA matrix in PC-I,[25,26] and to extensive reaction between the functional groups of the PLA and those of the rubber in PI-C, and to the enhanced clay dispersion in both of these nanocomposites as evaluated by XRD and TEM. However, the low tensile strengths of CI-P and ALL-S are due to the encapsulation of most of the clay inside the rubber. Moreover, the agglomerates in CI-P, especially at 15 wt % rubber content, might have acted as stress concentrators facilitating easy initiation and propagation of microcracks and leading to premature failure.[11,12,17,22]

When the rubber content reached 20 wt %, the tensile strength underwent a drastic drop in all the mixing protocols that could be due to the considerable softening effect induced by the rubber that hindered the benefits of the OMMT.[6,8]

Elongation at Break

Figure 9 illustrates the effect of rubber and clay addition on the elongation at break (ε_b) of the prepared nanocomposites. PLA is a stiff and brittle material, therefore as expected, it displayed low extensibility of 3.9% with slight stress whitening around the broken surfaces indicating that PLA deformed primarily by crazing mechanism,[6,9,10] and because of the absence of craze stoppers and/or craze diverting processes, the crazes that formed during extension grew and coalesced rapidly to form catastrophic cracks that resulted in premature breakup with low energy consumption and limited deformation.

Upon inclusion of 2 wt % OMMT into PLA, the tensile strain at break increased to 5.1% with substantial stress whitening on the specimen surfaces exhibiting higher degree of crazing and toughness enhancement. This result is in line with nanofiller reinforced impact modified PLA.[11,15] This slight increase in PLA drawability is attributed to intercalated/partially exfoliated dispersion of clay that promotes effective crack deflection that lengthens crack propagation paths and retards crack growth to fatal cracks.[6,29] Furthermore, the strong interfacial adhesion that

results from interactions between the functional groups of PLA and those of the OMMT enables efficient load transfer between the phases. However, this improvement was low due to the presence of tactoids as detected by XRD and TEM, and likely to the low OMMT content (2 wt %).

For all the mixing methods, when the rubber was incorporated to PLA/OMMT, all of the formulations displayed higher ε_b than pristine PLA with extensive stress whitening throughout the specimens induced by large amount of crazes giving rise to ductile deformation. The increase in tensile strain at break can be attributed to the high flexibility of the elastomer and to the effective stress transfer between the PLA and the rubber owing to the strengthened interface by the *in situ* formed PLA-g-rubber copolymer at the interface via the chemical reaction between the PLA and the rubber functional groups. The energy dissipation and high extension stemmed from a combination of massive crazes observed on the specimens and debonding/cavitation of the rubber particles as observed by SEM. Cavitation occurs during debonding and results in plastic deformation of the matrix and energy dissipation that improves tensile toughness.[2,7–11,15,30] This increase in elongation at break due to rubber addition is consistent with results published on rubber-toughened PLA.[1–8,10,11,13,15]

The ε_b attained a maximum at 10 wt % rubber fraction for all the preparation protocols without significant sacrifice of strength and toughness, but beyond this rubber content it declined steadily. The highest ε_b observed for PI-C and PC-I at this rubber loading is attributed to enhanced clay dispersion and to small rubber phase size in these mixing orders as observed by SEM. PI-C showed higher ε_b than PC-I did, due to the higher intermolecular reaction between the end groups of PLA and rubber in this mixing order compared with PC-I. The low ε_b for ALL-S and CI-P mixing orders might be due to the location of the clay in the dispersed phase in these nanocomposites that reduced rubber toughening efficiency by hindering its cavitation ability, and to the large rubber particle size as determined by SEM.

Beyond 10 wt % rubber content, the ε_b decreased considerably in all the preparation sequences owing to the presence of clay tactoids for PI-C and ALL-S and even agglomerates for CI-P that might have acted as flaws and defects, and to increased rubber domain size as observed by SEM. Because of the high difference in modulus between the rubber and the matrix, these large rubber domains might have acted as stress concentration points causing microdamages to develop readily to fatal cracks that lead to low ε_b.[3,4,8,11,15] When the rubber quantity reached 20 wt %, the ε_b dropped below 20% for all the nanocomposites.

Impact Strength

Figure 10 exhibits the effect of mixing sequences on unnotched Charpy impact strength (IS) as a function of rubber loading. As expected, neat PLA failed in a brittle manner with a recorded IS of only 18.4 J/m^2. Addition of 2 wt % OMMT to PLA reduced its IS to 17.0 J/m^2. This is a well-known fact, that is, the stiffness and strength improvement in nanocomposites is generally accompanied with a reduction in fracture-toughness. This slight reduction in impact toughness is due to the constraining effect

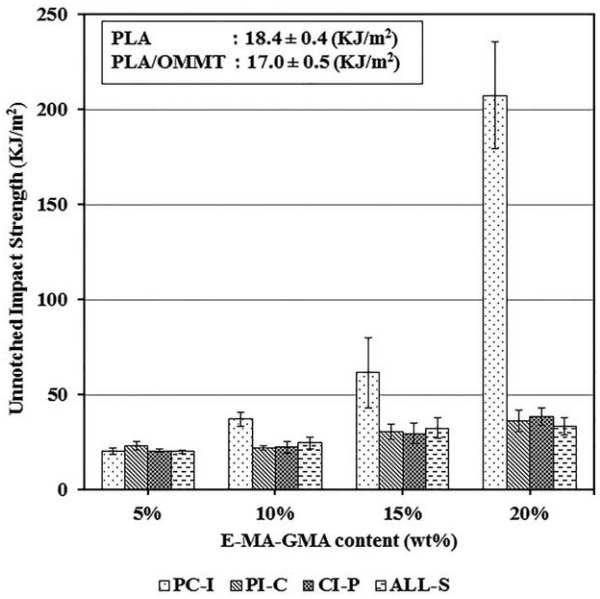

Figure 10. Unnotched Charpy impact strength of the ternary nanocomposites as a function of rubber content at 2 wt % clay.

of the OMMT on molecular mobility, and to the absence of efficient toughening mechanisms such as crack-tip blunting and crack bridging encountered in fracture processes of traditional polymer micro-composites, because the intercalated/partially exfoliated nanosheets are unable of producing such energy dissipating mechanisms.[30] Another reason for the decline in IS can also be assigned to the presence of tactoids in the PLA/OMMT nanocomposite as revealed by XRD and TEM analyses. These tactoids act as stress raisers and lead to early failure.[22,23] However, the decrease in IS was not high, because the effects of the negative factors are counteracted by the effective interactions between the clay nanoplatelets and PLA contributing to enhanced load transfer between the matrix and the nanoreinforcement.

For all the preparation procedures, the IS was gradually improved as the rubber fraction increased from 5 to 20 wt % [Figure 10]. This correlates with the elastomeric nature of the rubber and with the *in situ* formation of graft copolymer (PLA-g-rubber) at the interface. This copolymer situated at the interface promotes load transfer, consequently improving the IS. In addition, the homogeneous dispersion of the rubber domains initiates multiple crazes (as observed by the intense stress whitening on fractured specimens) and stops and/or deflects the crazes and cracks giving rise to efficient strain energy dissipation responsible of enhanced IS. This improvement of IS owing to addition of the low stiffness-low strength E-MA-GMA rubber to PLA corroborates with the results of different research studies.[1,2,4–8,11,15,17,18,20,22–26]

At 5 wt % rubber concentration, all of the nanocomposites displayed similar IS of nearly 20.0 J/m^2. However, at 10 wt % and higher rubber content, the PC-I nanocomposites exhibited the highest IS owing to their small rubber domain size and to superior clay dispersion, as detected by XRD and TEM techniques. Especially, above 10 wt % rubber content high degree of clay

Table I. Calorimetric Characteristics of PLA and its Nanocomposites

	T_g (°C)	T_c (°C)	T_m (°C)	χ_c (%)
PLA	56.13	115.79	147.07	5.94
PLA/OMMT, Clay (2 wt %)	57.20	109.40	150.74	3.70
PC-I, Rubber (wt %)				
5	58.55	102.76	149.30	4.42
10	57.44	102.93	148.25	5.78
15	58.28	104.52	147.51	7.20
20	57.58	108.58	148.11	7.82
PI-C, Rubber (wt %)				
5	58.89	104.12	149.08	4.39
10	58.96	103.38	148.09	4.88
15	57.45	103.78	147.58	5.08
20	57.70	103.90	145.07	6.26
CI-P, Rubber (wt %)				
5	57.39	105.79	146.44	3.92
10	57.08	105.38	145.92	6.10
15	55.98	107.48	146.20	7.05
20	57.55	110.51	150.58	7.62
ALL-S, Rubber (wt %)				
5	58.70	104.26	146.13	4.07
10	59.16	105.28	145.91	5.51
15	58.91	105.01	146.34	5.99
20	58.71	105.78	146.66	7.62

dispersion was achieved resulting in favorable impact resistance enhancement. Furthermore, the likely presence of most of the clay in the PLA continuous phase, as discussed earlier, should be another important factor for the high IS recorded for PC-I nanocomposites.[25,26]

A super tough PC-I nanocomposite was obtained at 20 wt % rubber content with an IS above 207.3 J/m^2 representing 11-fold increase compared with that of neat PLA. The PC-I specimens with 10 and 15 wt % rubber content were partially broken, whereas some of the specimens with 20 wt % rubber did not break, but only bended indicating that the actual IS would be greater than 207.3 J/m^2.

PI-C, CI-P, and ALL-S nanocomposites displayed almost similar IS at all rubber contents, and this value was lower than that of the IS of PC-I owing to their larger rubber particle size compared with PC-I. Large rubbery domain size increase stress concentration effects, thus reducing the beneficial effect of the rubber. The results on IS demonstrate that, especially for PI-C and PC-I, at 10 wt % stiffness-toughness balance was accomplished.

Thermal Analyses

DSC was performed to investigate the thermal behavior of PLA and its nanocomposites. The DSC data were determined from only one heating scan (0–200°C), because the crystallinity of PLA in the as molded specimens would affect the mechanical performance of the nanocomposites, and the goal was to find the crystallinity of the tensile samples. PLA and the nanocomposites exhibited similar thermograms (not shown here) characterized by three prominent transitions namely: a glass transition temperature (T_g), a crystallization exotherm (T_c and ΔH_c), and a melting endotherm (T_m and ΔH_m). Values of these relevant thermal properties derived from the thermograms are shown in Table I including the estimates of the degree of crystallinity (χ_c) of PLA computed using eq. (3) and a value of 93 J/g for the heat of fusion of 100% crystalline PLA.[3,8]

The T_g of PLA was clearly observed on all the DSC traces and that of the rubber which is below room temperature was not detected by this DSC analysis, consequently it was not studied here. The pure rubber shows only a melting temperature (T_m) recorded at 53.10°C. Neat PLA had a T_g centered at 56.13°C, a crystallization peak T_c at 115.79°C and a subsequent melting peak T_m at 147.07°C. The areas of the crystallization and melting peaks on its thermogram were almost the same indicating that PLA was primarily in the amorphous state after the injection process. This was also confirmed through its computed degree of crystallization using eq. (3) ($\chi_c \approx 5.94\%$).

As can be noticed from Table I, neither clay and rubber addition nor the blending protocols and rubber fraction significantly affected the T_g of PLA in the nanocomposites suggesting that after blending the macromolecular chains conserved their mobility and that the PLA and the rubber were immiscible.[8,16] Interestingly, T_m of all the nanocomposites also remained relatively unchanged with variations of about only 1–3°C implying that the rubber and the clay did not significantly modify the PLA crystal structure and did not affect the integrity of its crystals.[1] Unaltered T_g after OMMT and rubber addition to PLA was observed in various studies[6,11,14] and similar results were also found by Chow et al.[15] for PLA/SEBS-g-MA/nanoprecipitated $CaCO_3$ (NPCC), and by Alyamac and Yilmazer[21] for PET/E-MA-GMA/OMMT nanocomposites.

There was a substantial shift to lower temperature of the PLA crystallization transition peaks (Table I). The T_c of PLA decreased from 115.79 to 109.40°C after addition of 2 wt % OMMT showing that clay served as a heterogeneous nucleating agent.[6,11–14,16,17] The nucleating effect of OMMT was more significant in the case of PC-I, PI-C and ALL-S nanocomposites owing to their high clay dispersion level (high aspect ratio) and high contact area that are favorable for crystal nucleation. In a previous work on PET/E-MA-GMA/OMMT, a decrease of T_c from 138 to 128°C was detected at 1 wt % OMMT. The decrease in T_c was more significant at higher clay contents, and this decrease in T_c was found to be independent of the compounding sequence of the nanocomposites and it was attributed to the nucleating effect of OMMT.[21]

Regardless of the mixing order, addition of the rubber in all the nanocomposites induced a further decrease in T_c (Table I) pointing out to the nucleating activity of the rubber.[6,16] The T_c of PLA decreased after being toughened by an ethylene copolymer (Biostrong from DuPont), and then underwent a progressive decrease as the clay content increased. This effect was attributed to the nucleating behavior of both clay and

Biostrong.[17] Dasari et al.[25] also reported the nucleating effect of SEBS-g-MA in binary PA66/SEBS-g-MA blend, before incorporation of OMMT. The thermal results reported here (T_g, T_m, T_c) are also in line with those obtained by Balakrishnan et al.[17] It was reported that T_g and T_m were unchanged after Biostrong and clay addition; whereas both of these additives were found to exert strong nucleating effect on PLA and reduced its T_c.

According to Table I, significant decrease in T_c is observed for PC-I, because it was in this compounding order that the clay was best dispersed and the clay mostly resided in PLA phase permitting the clay to serve as effective heterogeneous nucleating agent for PLA. The lowest drop in T_c was recorded for CI-P probably due to confinement of most of the clay particles inside the rubber phase which therefore blocked its ability to act as nucleating species.[11,14] In the study of PLA/SEBS-g-MA/NPCC, Chow et al.[15] found that the nucleating effect of the NPCC was inhibited owing to its embedment in the rubber.

The degree of crystallinity (χ_c) of PLA decreased slightly from 5.94 to 3.70% after incorporation of OMMT to PLA, because the clay imposed restrictions to chain motion necessary for crystallization.[6,11,13,18,23] For all the mixing sequences there was a slight increase in χ_c as the rubber loading increased, but the level of crystallinity was less than 8%.

Finally, it can be stated that the interfacial strength associated with the effective physical and chemical interactions between the phases were the key factors for tensile and impact properties that were highly affected by the compounding protocol, clay dispersion and size of the rubber domains. However, in the present study, all of the nanocomposites had nearly comparable low crystallinity levels in the range of 4–8% irrespective of the preparation sequence. Thus, the crystallinity did not significantly affect the mechanical properties in this study.

CONCLUSIONS

PLA was reactively melt blended with an E-MA-GMA rubber in the presence of 2 wt % of an OMMT. The rubber content was varied from 5 to 20 wt % and four components addition protocols were used to prepare the nanocomposites in a co-rotating twin screw extruder.

XRD results, which were confirmed by TEM, revealed that PC-I resulted in the best clay dispersion and CI-P resulted in the worst one. Complete exfoliation of OMMT was not achieved, and all of the nanocomposites exhibited intercalated/partially exfoliated structures.

SEM observations revealed that PLA and the rubber were immiscible, but compatible attributed to the effective chemical reaction between the functional groups of the polymers. The rubber formed sub-micron dispersed phase, the size of which was influenced by the preparation procedure. PC-I and PI-C nanocomposites exhibited the smallest rubber particle size associated with their superior clay dispersion and with the active role of clay that acted as a barrier for coalescence, whereas ALL-S and CI-P nanocomposites showed larger phase size as a result of the encapsulation of most of the clay in the rubber, which hindered the barrier effect of clay for coalescence and reduced droplet breakup by stiffening the rubber. Incorporation of the rubber into the nanocomposites resulted in debonding/cavitation, crazing and shear yielding energy dissipating mechanisms in all of the nanocomposites and changed PLA deformation behavior from brittle to ductile.

Mechanical performance of the nanocomposites was influenced by the mixing sequence. The rubber and OMMT addition improved ductility and toughness of PLA without significantly sacrificing the strength, and optimum stiffness-fracture toughness was achieved at 10 wt % rubber content. PC-I nanocomposites showed the highest impact toughness and PI-C nanocomposites exhibited the highest elongation at break in tensile tests, owing to their better clay dispersion and their small rubber particle size. ALL-S and CI-P displayed lower mechanical performance than the PC-I and PI-C, because of their large particle size and reduced rubber cavitation ability due to the encapsulation of most of the clay in the rubber in these nanocomposites.

DSC analyses confirmed the immiscibility of the blended polymers. After addition of rubber and OMMT to PLA, T_g and T_m of the matrix remained relatively unaltered, but T_c underwent a substantial decrease demonstrating the heterogeneous nucleating role of the elastomer and the clay. These thermal characteristics and the degree of crystallinity were found to be independent of the preparation procedure.

REFERENCES

1. Zeng, J.; Li, Y.; He, Y.; Li, S.; Wang, Y. *Ind. Eng. Chem. Res.* **2011**, *50*, 6124.
2. Zhao, Q.; Ding, Y.; Yang, B.; Ning, N.; Fu, Q. *Polym. Test.* **2013**, *32*, 299.
3. Yeh, J.; Tsou, C.; Li, Y.; Xiao, H.; Wu, C.; Chai, W.; Lai, Y.; Wang, C. *J. Polym. Res.* **2012**, *19*, 9766.
4. Juntuek, P.; Ruksakulpiwat, C.; Chumsamrong, P.; Ruksakulpiwat, Y. *J. Appl. Polym. Sci.* **2012**, *125*, 745.
5. Sun, S.; Zhang, M.; Zhang, H.; Zhang, X. *J. Appl. Polym. Sci.* **2011**, *122*, 2992.
6. Baouz, T.; Rezgui, F.; Yilmazer, U. *J. Appl. Polym. Sci.* **2013**, *128*, 3193.
7. Zhang, N.; Wang, Q.; Ren, J.; Wang, L. *J. Mater. Sci.* **2009**, *44*, 250.
8. Taib, R. M.; Ghaleb, Z. A.; Mohd Ishak, Z. A. *J. Appl. Polym. Sci.* **2012**, *123*, 2715.
9. Bhardwaj, R.; Mohanty, A. K. *Biomacromolecules* **2007**, *8*, 2476.
10. Meng, B.; Deng, J.; Liu, Q.; Wu, Z.; Yang, W. *Eur. Polym. J.* **2012**, *48*, 127.
11. Leu, Y. Y.; Mohd Ishak, Z. A.; Chow, W. S. *J. Appl. Polym. Sci.* **2012**, *124*, 1200.
12. Balakrishnan, H.; Hassan, A.; Wahit, M. U.; Yussuf, A. A.; Abdul Razak, S. B. *Mater. Des.* **2010**, *31*, 3289.
13. Yu, Z.; Yin, J.; Yan, S.; Xie, Y.; Ma, J.; Chen, X. *Polymer* **2007**, *48*, 6439.

14. Chow, W. S.; Lok, S. K. *J. Therm. Anal. Calorim.* **2009**, *95*, 627.
15. Chow, W. S.; Leu, Y. Y.; Mohd Ishak, Z. A. *Express Polym. Lett.* **2012**, *6*, 503.
16. Lewitus, D.; McCarthy, S.; Ophir, A.; Kenig, S. *J. Polym. Environ.* **2006**, *14*, 171.
17. Balakrishnan, H.; Masoumi, I.; Yussuf, A. A.; Imran, M.; Hassan, A.; Wahit, M. U. *Polym-Plast. Technol.* **2012**, *51*, 19.
18. Ahn, Y.; Paul, D. R. *Polymer* **2006**, *47*, 2830.
19. Coskunses, F. I.; Yilmazer, U. *J. Appl. Polym. Sci.* **2011**, *120*, 3087.
20. Yeniova, C. E.; Yilmazer, U. *Polym. Comp.* **2010**, *31*, 1853.
21. Alyamac, E.; Yilmazer, U. *Polym. Comp.* **2007**, *28*, 251.
22. Martins, C. G.; Larocca, N. M.; Paul, D. R.; Pessan, L. A. *Polymer* **2009**, *50*, 1743.
23. Borah, J. S.; Karak, N.; Chaki, T. K. *Mat. Sci. Eng. A* **2011**, *528*, 2820.
24. Oliveira, A. D.; Larocca, N. M.; Paul, D. R.; Pessan, L. A. *Polym. Eng. Sci.* **2012**, *52*, 1909.
25. Dasari, A.; Yu, Z.; Yang, M.; Zhang, Q.; Xie, X.; Mai, Y. *Comp. Sci. Tech.* **2006**, *66*, 3097.
26. Dasari, A.; Yu, Z.; Mai, Y. *Polymer* **2005**, *46*, 5986.
27. Hong, J. S.; Namkung, H.; Ahn, K. H.; Lee, S. J.; Kim, C. *Polymer* **2006**, *47*, 3967.
28. Oyama, H. T.; Kitagawa, T.; Ougizawa, T.; Inoue, T.; Weber, M. *Polymer* **2004**, *45*, 1033.
29. Balakrishnan, S.; Start, P. R.; Raghavan, D.; Hudson, S. D. *Polymer* **2005**, *46*, 11255.
30. Lim, S.; Dasari, A.; Yu, Z.; Mai, Y.; Liu, S.; Yong, M. S. *Comp. Sci. Tech.* **2007**, *67*, 2914.
31. Pillin, I.; Montrelay, N.; Bourmaud, A.; Grohens, Y. *Polym. Degrad. Stab.* **2008**, *93*, 321.
32. Zenkiewicz, M.; Richert, J.; Rytlewski, P.; Moraczewski, K.; Stepczynska, M.; Karasiewicz, T. *Polym. Test.* **2009**, *28*, 412.